

Shroom regulates epithelial cell shape via the apical positioning of an actomyosin network

Jeffrey D. Hildebrand

Department of Biological Sciences, 4249 Fifth Avenue, Crawford Hall, University of Pittsburgh, Pittsburgh, PA 15260, USA
e-mail: jeffh@pitt.edu

Accepted 9 August 2005
Journal of Cell Science 118, 5191-5203 Published by The Company of Biologists 2005
doi:10.1242/jcs.02626

Summary

The actin-binding protein Shroom is essential for neural tube morphogenesis in multiple vertebrate organisms, indicating its function is evolutionarily conserved. Shroom facilitates neurulation by regulating the morphology of neurepithelial cells. Shroom localizes to the apical tip of adherens junctions of neural ectoderm cells *in vivo* and to the apical junctional complex (AJC) in MDCK cells. Induced expression of Shroom in polarized epithelia elicits apical constriction and dramatic reorganization of the apical arrangement and packing of cells without altering apical-basal polarity. These events likely mimic the cell shape changes and cellular movements required for neurulation *in vivo*. The observed phenotypes depend on

the ability of Shroom to alter F-actin distribution and regulate the formation of a previously uncharacterized contractile actomyosin network associated with the AJC. Targeting the C-terminal domain of Shroom to the apical plasma membrane elicits constriction and reorganization of the actomyosin network, indicating that this domain mediates Shroom's activity. *In vivo*, Shroom-mutant neural epithelia show a marked reduction in apically positioned myosin. Thus, Shroom likely facilitates neural tube closure by regulating cell shape changes via the apical positioning of an actomyosin network in the neurepithelium.

Key words: Shroom, Neural tube, Myosin II, Epithelial, Constriction

Introduction

One of the most intensely studied populations of morphogenic epithelia is that which gives rise to the adult brain and spinal chord, as defects in neural tube closure affect approximately 0.1% of human births, resulting in spina bifida and anencephaly (Campbell et al., 1986; Copp et al., 1990a). The neural tube is generated from polarized ectodermal epithelium that undergoes a series of well-defined morphogenetic movements that convert the flat neural plate into the closed neural tube (Colas and Schoenwolf, 2001). This conversion is driven by a combination of intrinsic and extrinsic forces (Smith and Schoenwolf, 1997). The actin cytoskeleton appears critical for generating some or all of the requisite intrinsic forces, while the surrounding tissues provide the necessary extrinsic forces.

In the neural epithelium actin is predominantly localized in a dense band that encircles each cell at the apical tip of the adherens junction. Contraction of this ring may convert columnar epithelial cells into wedge-shaped cells with narrower apical surfaces. Such alterations in cell shape would facilitate the formation of the medial and dorsolateral hinge-points. These morphologically distinct domains of the neural epithelium are necessary for elevation of the neural folds and juxtaposition of the lateral edges of the neural fold at the future dorsal midline (Smith and Schoenwolf, 1997). Since neural epithelial cells are attached to each other by adhesions receptors, such as cadherins, nectins and JAM (Okabe et al., 2004; Takekuni et al., 2003), the cumulative effects of the contractile forces exerted in the apical domain of each individual cell would generate a 'purse-string' working to close the neural tube. In addition to altering cell shape, this actin

network appears essential for maintaining tension across the apical surface of the neural epithelium and provides the tissue rigidity necessary to successfully complete morphogenesis (Ybot-Gonzalez and Copp, 1999).

Evidence for the importance of proper F-actin organization and regulation during neural tube closure comes from experiments using both genetic and pharmacological approaches. Treatment of embryos with cytochalasin D prevents cranial neural tube closure (Schoenwolf et al., 1988; Ybot-Gonzalez and Copp, 1999). These results are supported by the genetic ablation in mice of numerous actin-associated proteins or modulators of actin dynamics, including *shroom* (Hildebrand and Soriano, 1999), *vinculin* (Xu et al., 1998), *Menalprofilin* (Lanier et al., 1999; Menzies et al., 2004), *p190RhoGAP* (Brouns et al., 2000), *marcks* (Stumpo et al., 1995) and *arglabl* (Koleske et al., 1998). Mutations in all of these genes result in neural tube defects of varying severity.

In non-muscle cells, actomyosin-based contractility regulates numerous processes, including morphology, cytokinesis and motility. All of these utilize the non-muscle myosin II heavy chain, the activity of which is regulated through phosphorylation of either the heavy chains or the regulatory myosin light chains (RMLC) (Bresnick, 1999; Redowicz, 2001). Phosphorylation of the RMLC is positively regulated by the activities of the Rho-associated kinase (Rock) and myosin light chain kinase, and negatively regulated by the myosin phosphatase (Bresnick, 1999). While much of this work has utilized *in vitro* cell culture systems, the importance of this pathway in tissue morphogenesis during vertebrate development has been demonstrated by targeted ablation in

mice of *rock I* and *rock II* (Shimizu et al., 2005; Thumkeo et al., 2003). In addition, this pathway seems essential for elaborating striated layers of keratinocytes in vitro (Vaezi et al., 2002). In both of these systems, Rock, acting through myosin II, organizes the formation of actin cables that facilitate cellular and tissue morphogenesis. A role for this pathway in neurulation comes from the observation that treatment of embryos with the Rock inhibitor Y-27632 causes defects in neural tube morphogenesis (Wei et al., 2001).

The actin-binding protein Shroom (Shrm) is required for proper closure of the neural tube in mice and *Xenopus* (Haigo et al., 2003; Hildebrand and Soriano, 1999). Shrm exerts its influence by inducing cells to constrict their apical surfaces and change their morphology. This study describes the mechanism by which Shrm regulates apical architecture in polarized epithelial cells. Shrm controls the cellular distribution of contractile actomyosin both in cell culture and in the developing mouse embryo. These data suggest that Shrm may function at a critical regulation point for controlling cellular and tissue morphology during embryogenesis.

Materials and Methods

Cell culture

T23 MDCK cells were maintained in EMEM supplemented with 10% FBS (Hyclone), L-glut, and penicillin/streptomycin at 37°C and 5% CO₂. Cells were removed from the plates using Trypsin-EDTA and passaged every 2-3 days. T23 MDCK cells stably expressing the Tet-transactivator have been described previously (Barth et al., 1997). To generate MDCK cells with regulated expression of ShrmL and Endolyn-ShrmC (Endo-ShrmC), T23 MDCK cells were transfected with pTRE2-hyg-ShrmL or pTRE2-hyg-Endo-ShrmC (see below) using Lipofectamine 2000 (Invitrogen) and selected in media containing hygromycin (200 µg/ml, Invitrogen), G418 (300 µg/ml total drug, Gibco-BRL) and doxycycline (40 ng/ml, Sigma) for 8-10 days. Isolated colonies were expanded and screened for regulated expression of ShrmL or Endo-ShrmC. For drug treatment studies, cells were plated onto Transwell filters in the absence or presence of doxycycline for 24-48 hours. Cells were treated with either DMSO (vehicle), the ML-7 (40 µg/ml, Roche), Y-27632 (5, 10, or 20 µg/ml, Roche), or ±blebbistatin (50 or 100 µg/ml, CalBiochem) for 90 minutes or cytochalasin D (0.5, 1, or 2 µg/ml, Sigma) for 30 minutes at 37°C in the absence or presence of doxycycline. For transient transfection of cells on filters, cells were plated at a density of 3×10⁵ cells per well and grown for 24 hours. Cells were transfected with the DNA of interest (1 µg) using Lipofectamine 2000 and grown for 24 hours prior to processing.

For growth of cysts in collagen gels, either un-induced or induced ShrmL cells were trypsinized and resuspended at a concentration of 2×10⁴ cells/ml in collagen gel mix with or without doxycycline (1×DMEM, 2.5 mg/ml collagen, 2.3 mg/ml NaHCO₃ and 20 mM Hepes pH 7.4). Cells were plated in 12 well plates (500 µl/well) and allowed to solidify at 37°C. Gels were covered with 1 ml culture media with or without doxycycline and grown for 10 days with media changes every 2-3 days.

Molecular biology

pCS2 derivatives of ShrmL and ShrmS were described previously (Hildebrand and Soriano, 1999). To generate pCS2-Shrm1376-1986, pCS2-ShrmS was digested with *NcoI* and religated. To generate pCS2-Endo-ShrmC, a portion of the *endolyn* cDNA encoding amino acids 1-187 was amplified using Pfu polymerase and thermal cycling with primers that added 5' and 3' *NcoI* sites. The product was digested with *NcoI* and ligated into pCS2-Shrm1372-1986 that had been

digested with *NcoI*. pCS2-Endo-ShrmΔ was made by digesting pCS2-Endo-ShrmC with *EcoRI* and religating, resulting in a cDNA that encodes Endolyn and amino acids 1372-1572 of ShrmL. pTRE-ShrmL and pTRE-Endo-ShrmC were generated by cloning cDNAs encoding ShrmL and Endo-ShrmC from pCS2 into pTRE2-hygro (Clontech). Expression vectors for GFP-RhoA and GFP-RhoA19N (dominant negative) were described previously (Cetin et al., 2004).

Antibody staining, histology and western blotting

Shrm antibody UPT132 was generated by injecting rabbits with purified His-Shrm1472-1986. Shrm-specific antibodies were affinity purified using GST-Shrm1472-1986. The following antibodies were used: chicken anti-Shrm (Hildebrand and Soriano, 1999), Rat anti-ZO1 (1:400, Chemicon), mAb anti-E-cadherin (1:400 dilution, Transduction Labs), mAb anti-β-catenin (1:400, Transduction Labs), rabbit anti-non-muscle myosin II-B (1:250, Covance), mouse anti-myosin II CMII 23 (1:100, Development Studies Hybridoma Bank), rabbit anti-di-phospho myosin light chain (1:25, Cell Signaling) and rat anti-nectin-3 (1:100, provided by Takei, Osaka, Japan). Primary antibodies were detected using Alexa-488, -568 and -633 conjugated secondary antibodies (1:400 dilution, Molecular Probes). F-actin was visualized with TRITC or Alexa-633 conjugated phalloidin (Sigma and Molecular Probes, respectively).

For immunofluorescent staining of cells, samples were fixed using either -20°C methanol for 5 minutes, 4% paraformaldehyde (PFA) in PBS for 15 minutes, or the pH shift protocol (Apodaca et al., 1994). Fixed cells were stained with primary antibody for 1 hour at RT, washed in PBT three times for 5 minutes at room temperature, stained with secondary antibody for 1 hour at room temperature, washed as above and mounted using VectaShield (Vector Labs).

For staining of embryo sections, embryos were isolated at the indicated developmental time point and stained as previously described (Hildebrand and Soriano, 1999). All mice used for the derivation of embryos were on a C57Bl/6 background. Embryos were isolated from timed mating of *shrm*-heterozygous mice (Hildebrand and Soriano, 1999). For comparative analysis, wild type and *shrm* mutant littermates were embedded side-by-side, sectioned together and stained on the same slide. Results are representative of three experiments from three different litters.

For staining cysts, gels were washed extensively with PBS and removed from wells. Gels were cut into pieces and washed with PBS in 2 ml tubes. Gels were treated with Collagenase, type VII (Sigma) for 10 minutes at 37°C, washed in PBS and fixed in 4% PFA for 30 minutes at RT with constant rocking. Fixation was quenched with 75 mM NH₄Cl and 20 mM Glycine (pH 8.0) in PBS. Gels were then blocked in PFS (PBS supplemented with 0.7% fish skin gelatin, 0.025% saponin) for 30 minutes and incubated in primary antibody diluted in PFS for 12 hours at 4°C with constant rocking in 2 ml tubes. Gels were washed three times for 15 minutes at RT in PFS and then incubated in secondary antibodies or phalloidin diluted in PFS for 12 hours at 4°C. Gels were washed as above and mounted.

Images were acquired using a Biorad Radiance 2000 Laser Scanning System mounted on a Nikon E800 microscope (60× objective, NA 1.3). Collected images were processed using Adobe Photoshop and NIH Image. For cellular measurements, NIH Image was used to measure the area of a cell outlined by E-cadherin staining at the basal surface (a distance of 1.5 µm from the filter) and the apical surface (as defined by the distribution of ZO-1).

For western blotting, cells were lysed in RIPA buffer and 30 µg of total cell lysate was resolved by SDS-PAGE and transferred to nitrocellulose. Membranes were blocked in TBST/4% milk, probed with UPT132 (diluted 1:500 in TBST/4% milk) overnight at 4°C, washed in TBST three times for 5 minutes at RT and probed with HRP-conjugated secondary antibodies (Amersham) diluted 1:2500 in TBST/4% milk. Filters were washed as above and HRP detected using ECL reagent (Amersham).

Results

Shrm expression and subcellular distribution in the neural ectoderm

The actin-binding protein Shrm is required for neural tube closure and is thought to work through the actin cytoskeleton or cell adhesion complexes to regulate the apical morphology of cells in bending regions of the neural plate (Haigo et al., 2003; Hildebrand and Soriano, 1999). To test this hypothesis, cryosections of the neural epithelium from embryonic (e) 9.25 dpc mouse embryos were stained to detect Shrm during neural tube closure. Just prior to cranial closure, Shrm is found in a honeycomb array that is restricted to the apical tips of the lateral membranes of neuroepithelium (Fig. 1A). This array represents a circumferential ring located at the apical tip of the adherens junction and may be related to the apical junctional complex (AJC) observed in other types of polarized epithelia (Nelson, 2003). In single optical sections, this ring is represented as a discrete spot (arrowheads, Fig. 1B) that overlaps with the apical-most aspect of β -catenin, which distributes along the entire lateral membrane (arrows, Fig. 1B). This distribution of Shrm is observed along the entirety of both the dorsal-ventral and anterior-posterior axes of the neural ectoderm at this developmental stage. This suggests that Shrm function might be required in all neural epithelium during morphogenesis and not just that which is undergoing bending (Hildebrand and Soriano, 1999).

The distribution of Shrm in the neural epithelium is consistent with that of F-actin and proteins found in the AJC, including receptors such as Nectins, Occludins and JAM, and regulatory factors such as ZO-1, Par proteins and Afadin (Okabe et al., 2004; Takekuni et al., 2003; Vogelmann and Nelson, 2005). In most polarized epithelia, the AJC is localized at the apical portions of the lateral membrane and is a key determinant of cell adhesion, morphology and polarity (Nelson, 2003). To verify that Shrm localizes to this regulatory complex, embryo sections were co-stained to detect Shrm, F-actin and β -catenin (Fig. 1C) or Shrm and Nectin-3 (Fig. 1D). Shrm shows extensive co-localization with both F-actin and Nectin-3 (arrowheads, Fig. 1C,D). These results indicate that Shrm is restricted to the putative AJC in neuroectoderm and could participate with actin, adhesion complexes, or other cytoskeletal proteins to regulate cellular architecture during neurulation.

Shrm expression in MDCK cells alters cell morphology

As a way of modeling the role of Shrm in epithelial cell morphology, cell lines exhibiting tetracyclin regulated expression of full-length Shrm (ShrmL) were generated (ShrmL cells). Western blot analysis shows expression of a protein of the correct size following induction (Fig. 1E). To evaluate the subcellular distribution of

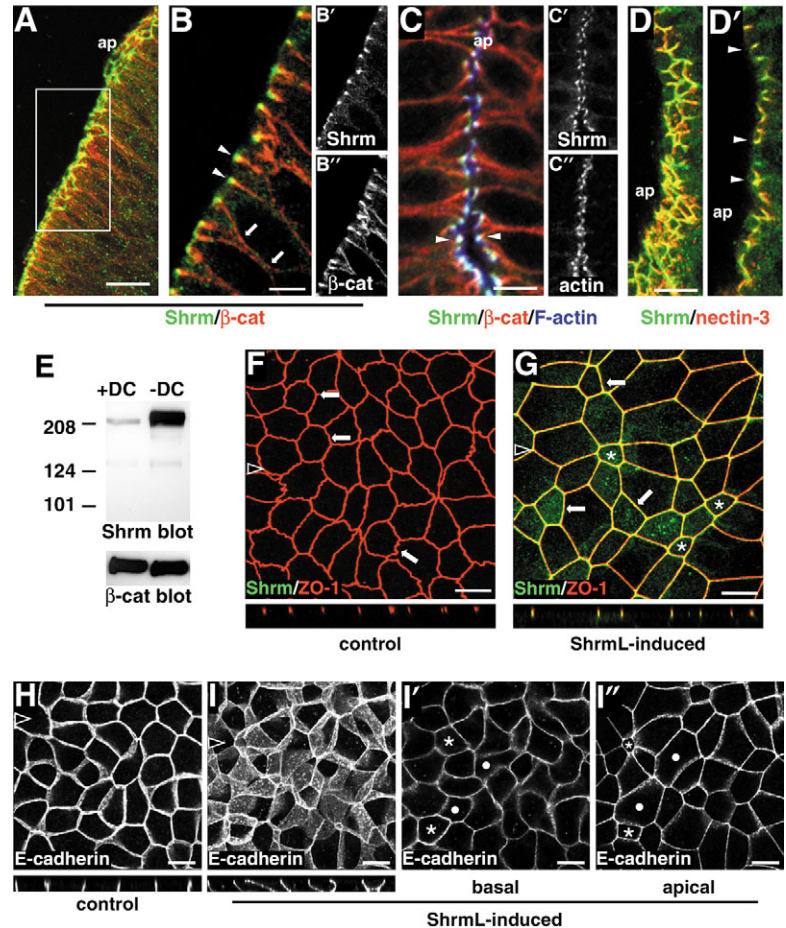


Fig. 1. Shrm is localized to the apical junctional complex (AJC).

(A) Cryosections from e9.25 embryos were stained to detect Shrm (green) and β -catenin (red). Shrm is distributed in an apically positioned honeycomb array in a projection of confocal sections. ap, apical. (B) An enlarged single optical section from the boxed region in panel A. Arrows indicate laterally positioned β -catenin (red) and white arrowheads indicate apically positioned Shrm (green). (C) Cryosections from the trunk region of an e9.5 embryo stained to detect Shrm (green, C'), β -catenin (red) and F-actin (blue, C'). White arrowheads indicate apically positioned Shrm and F-actin. (D) Cryosections of e9.5 mouse embryos stained to detect Shrm (green) and Nectin-3 (red). A projected image shows Shrm (green) and Nectin-3 (red) in a honeycomb array. A single optical section demonstrating the overlapping distribution of Shrm and Nectin-3 in the putative AJC (white arrowhead) is shown in D'. (E) Equal amounts (30 μ g) of total cell lysate from induced and un-induced ShrmL cells were assayed by western blot analysis using anti-Shrm sera. Filters were re-probed to detect β -catenin to verify equal protein loading. (F and G) ShrmL cells were grown on Transwell filters for 48 hours in the presence (F) or absence (G) of doxycycline and stained to detect Shrm (green) and ZO-1 (red). Top panels are X-Y projections and bottom panels are X-Z projections. Arrows indicate cells with rounded and polyhedral morphology. (H,I) ShrmL cells plated on Transwell filters were grown in the presence (H) or absence (I) of doxycycline for 48 hours and stained to detect E-cadherin. Top panels are projections in the X-Y dimension and bottom panels are X-Z projections. Panels I' and I'' show individual optical sections of E-cadherin staining at the level of the basal surface and the AJC, respectively. Asterisks, constricted cells; dots, stretched cells. In all panels, scale bar is 15 μ m, open arrowheads indicate the position at which X-Z projections were generated; ap, apical.

ShrmL and its impact on cell morphology, ShrmL cells were grown on Transwell filters for 48 hours in the presence

(control, Fig. 1F) or absence (induced, Fig. 1G) of doxycyclin and stained to detect ShrmL and ZO-1, a component of the AJC and tight junctions. Ectopic ShrmL co-distributes with ZO-1 in the AJC (Fig. 1G). Induced ShrmL cells display three phenotypes when compared with control cells (Fig. 1F versus 1G). First, ShrmL causes many of the cells to undergo apical constriction (asterisks, Fig. 1G). Second, there is a large variation in the apical area of these cells, as defined by ZO-1 staining. This is likely the result of cells increasing their apical area to compensate for those constricting their apical surface. Third, ZO-1 staining of control cells demonstrates that at the level of the AJC these cells possess a more rounded circumference and display wavy tight junctions (arrows, Fig. 1F). By contrast, ShrmL cells are more polyhedral in shape with tight junctions that appear straight and rigid, as if the cells are under tensions (arrows, Fig. 1G). Analysis of the fluorescent intensity of constricted and stretched cells indicates that both populations of cells express relatively equal amounts of ShrmL (not shown). These data indicate that ShrmL localizes to the AJC *in vitro* and *in vivo*, its expression alters tight junction architecture and it regulates apical morphology.

It is possible that Shrm's activity is not limited to the apical surface but extends along the apical-basal axis. To test this, control and induced ShrmL cells were stained to detect E-cadherin and imaged by confocal microscopy (Fig. 1H,I). Control cells possess a normal columnar shape with apical and basal surfaces of roughly the same area that are aligned with each other (Fig. 1H). By contrast, cells expressing ShrmL lose their normal columnar appearance and adopt a wedge-shaped morphology due to alterations in apical area (Fig. 1I). Individual optical sections taken at the basal and apical

surfaces of induced cells depict this phenotype more clearly. Induced cells have basal surfaces that are roughly the same size and are morphologically indistinguishable. At the apical surface, however, induced cells show dramatic differences in size with some cells showing decreased (asterisks) or increased (dots) apical dimensions. As a consequence of these changes in shape, many cells reorganize their intercellular interactions such that their apical and basal portions form cell-cell adhesions with different neighboring cells (Fig. 1I, dots and asterisks).

Shrm expression alters the apical cell-cell alignment, but not polarity, of MDCK cells

To quantify the activity of Shrm and to correlate the changes in cell shape with ShrmL expression, ShrmL-expressing cells were mixed with wild-type cells, grown on filters for 48 hours in the absence of doxycyclin and stained to detect ShrmL, ZO-1 and E-cadherin (Fig. 2A-C). In these cultures, ShrmL-expressing cells have constricted apical surfaces (asterisks) while their non-expressing neighbors have increased apical areas (dots) as defined by ZO-1 staining (Fig. 2A). To quantify this, mixed cultures were stained with E-cadherin, visualized by confocal microscopy and analyzed to determine the area of ShrmL-expressing cells in the basal and apical domains relative to those of non-expressing neighboring cells (Fig. 2B,C). All cells in the population have basal surfaces of approximately the same area, with ShrmL cells possessing an average basal area of $123.5 \pm 16 \mu\text{m}^2$ and wild-type cells have an average basal area of $129.2 \pm 21 \mu\text{m}^2$. By contrast, cells expressing ShrmL have an average apical area of $50.6 \pm 9.5 \mu\text{m}^2$ while neighboring wild-type cells have an apical area of $187.6 \pm 16 \mu\text{m}^2$. Wild-type cells that are not neighboring ShrmL-expressing cells have average basal and apical areas of $119.4 \pm 10.1 \mu\text{m}^2$ and $122.6 \pm 12.7 \mu\text{m}^2$, respectively. These results are depicted graphically in Fig. 2D.

In these experiments, ShrmL-expressing cells always arrange themselves into tightly packed clusters at the apical surface (Fig. 2A). This arrangement of cells is similar to what has been

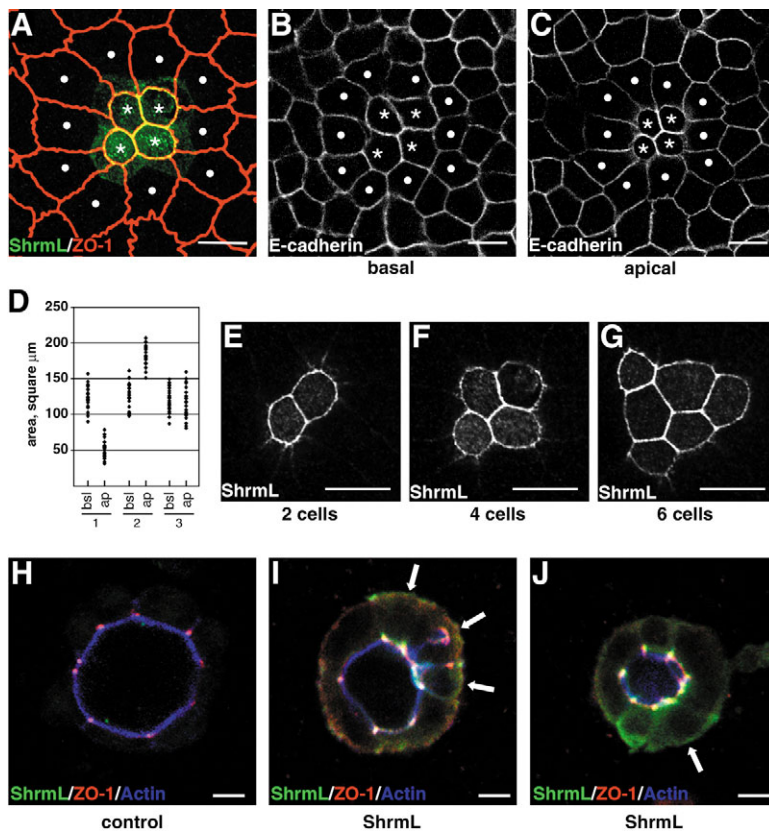


Fig. 2. Shrm controls apical morphology in MDCK cells. (A-C) A mixture of T23 and ShrmL cells were grown on Transwell filters in the absence of doxycyclin and stained to detect Shrm (green), ZO-1 (red) and E-cadherin (B,C). Asterisks indicate constricted, ShrmL-expressing cells and dots indicate stretched, non-expressing cells. Panels B and C show single optical sections of E-cadherin staining at the basal and apical surfaces, respectively. (D) Scatter plot of apical (ap) and basal (bsl) areas of ShrmL expressing (1), neighboring wild-type (2) and non-neighboring, wild-type (3) cells in mixed populations of ShrmL-expressing and wild-type T23 cells. Each point represents one cell. (E-G) Clusters of increasing numbers of ShrmL-expressing cells (stained to detect Shrm) show the configuration of cells at the level of the AJC. (H-J) Cysts generated from control cells (H) or induced ShrmL cells (I and J) were stained to detect Shrm (green), ZO-1 (red) and F-actin (blue). Arrows denoted cells with constricted apical surfaces. Scale bar represents $15 \mu\text{m}$ in all panels.

reported for the packing of cone cells in the ommatidia of the *Drosophila* compound eye (Hayashi and Carthew, 2004). Analysis of cell clusters of differing numbers of cells suggests that ShrmL expression causes the cells to arrange their apical domain to minimize surface area (Fig. 2E-G). Neither control nor ShrmL cells typically exhibit this arrangement in the lateral or basal domains. This packing arrangement may be the result of altered adhesive or tensile properties of these cells relative to their non-expressing neighbors. The phenotype of these mixed populations are different from what is observed in monolayers in which all cells are expressing Shrm in two ways (Fig. 1G). First, neighboring cells that increase their apical area do not display straight tight junctions. Second, in monolayers of mixed populations, all ShrmL-expressing cells are constricted. By contrast, in monolayers of induced ShrmL cells, expressing cells can be either stretched or constricted, indicating the whether a cell stretches or constricts is determined stochastically or by random chance. These observations suggests that Shrm is responsible for the altered appearance of tight junctions and that maintaining the integrity of the monolayer may be dominant to constriction, since if all cells constricted, the monolayer would likely be disrupted.

The results depicted above suggest that ShrmL expression changes cell shape and cellular organization, but does not alter the overall apical-basal polarity of cells. To assess this more stringently, un-induced or induced ShrmL cells were grown in collagen gels to facilitate the formation of cysts. Cysts were then stained to detect ShrmL, ZO-1 and F-actin. Both control cells and ShrmL cells form cysts that have a central lumen and exhibit normal distribution of actin and ZO-1 (Fig. 2H-J). However, cysts formed by ShrmL cells exhibit smaller central lumen and cells expressing higher levels of ShrmL have smaller apical areas (arrows, Fig. 2I and 2J). The lumens formed by ShrmL-expressing cells are approximately 40% smaller than those formed in control cysts ($275 \pm 34 \mu\text{m}^2$ versus $453 \pm 42 \mu\text{m}^2$, $n=20$ cysts composed of 8-10 cells at the equator of the cyst). In addition, the Shrm-expressing cells that have constricted apical areas also appear taller along the apical basal axis. This is also seen in the mixing experiment as indicated by the E-cadherin staining in the Shrm-expressing cells (Fig. 2C). These results show that ShrmL regulates cell shape and three-dimensional tissue architecture, but does not alter cellular polarity.

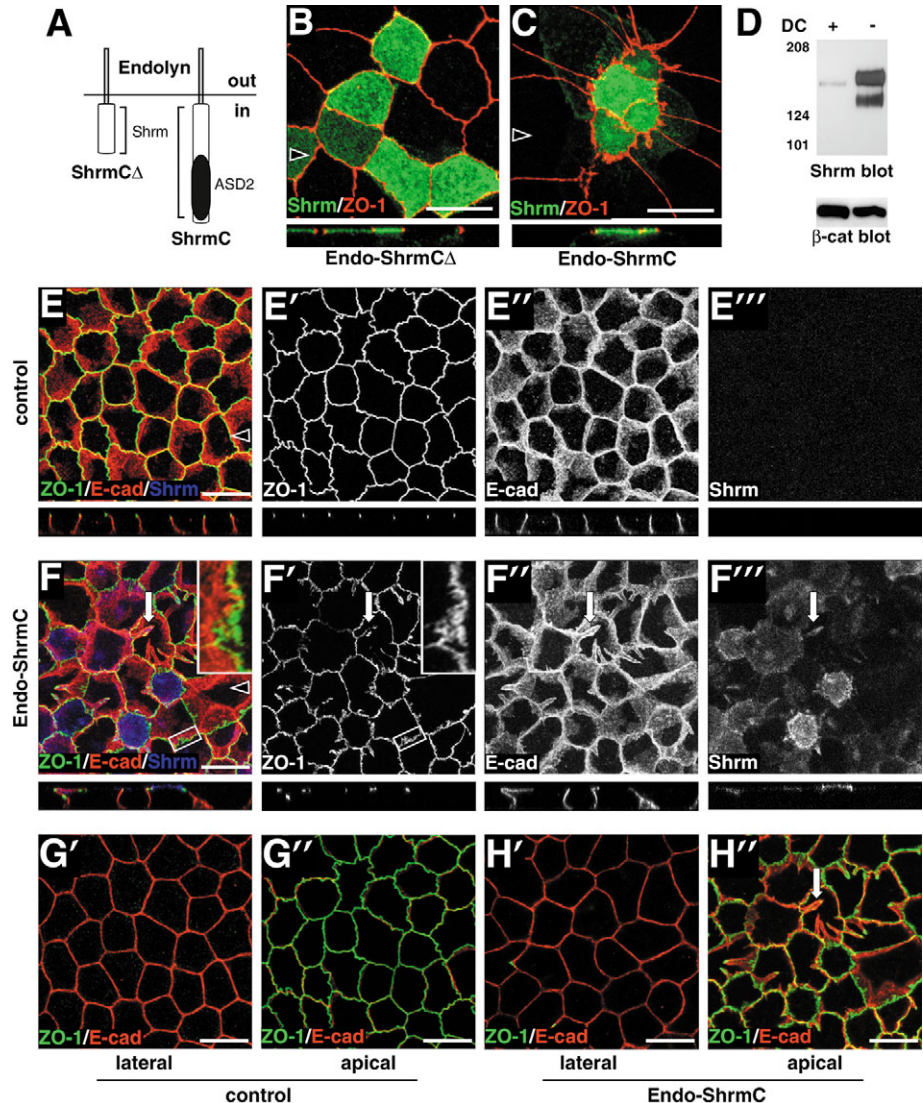
The C-terminal domain of Shrm regulates apical constriction

ShrmL contains three sequence motifs that are conserved in the other related family members: an N-terminal PDZ domain, a centrally located region termed ASD1 (Apx/Shrm Domain) and a C-terminal region termed ASD2 (Hildebrand and Soriano, 1999). Previous work has shown that Shrm requires both ASD1 and ASD2 to induce apical constriction and that Shrm can directly interact with F-actin through a portion of the protein containing ASD1 (Haigo et al., 2003; Hildebrand and Soriano, 1999). However, this actin-binding activity is not sufficient to cause apical constriction, as a Shrm protein consisting of the N-terminal 1264 amino acids targets correctly and binds actin but does not cause constriction (Haigo et al., 2003; Hildebrand and Soriano, 1999). This fostered the hypothesis that ASD1 and the actin-binding activity of Shrm

determine subcellular localization while ASD2 triggers apical constriction. To test this hypothesis, the C-terminal 614 amino acids of ShrmL (containing ASD2, amino acids 1372-1986) were targeted to an ectopic location to see if it was capable of altering the apical architecture of polarized cells. To this end, the C-terminus of Shrm was constitutively targeted to the apical surface of cells independent of any known actin-binding activity by generating a cDNA that expresses a chimeric protein consisting of the transmembrane protein Endolyn and the C-terminus of Shrm (Endo-ShrmC, Fig. 3A). A control protein consisting of Endolyn and amino acids 1372-1562 of ShrmL (lacking ASD2) was also expressed (Endo-ShrmCΔ). Endolyn was chosen because it traffics to the apical plasma membrane in MDCK cells and can be over expressed without altering cell morphology (Ihrke et al., 2001; Ihrke et al., 2000). When transiently expressed in MDCK cells these chimeric proteins are expressed at equivalent levels and traffic to the apical plasma membrane (Fig. 3B and 3C). While Endo-ShrmCΔ is inert, Endo-ShrmC potently induces apical constriction. Expression of the C-terminal domain of Shrm alone causes no phenotype and the protein is uniformly distributed in the cytoplasm (Haigo et al., 2003; Hildebrand and Soriano, 1999).

The activity of Endo-ShrmC was further tested using tetracycline-regulated expression in MDCK cells. Endo-ShrmC cells were generated and assayed for protein expression by western blotting. Induction results in expression of a protein that runs as a doublet of an apparent molecular mass of 150 kDa (Fig. 3D), which is larger than the predicted size of approximately 80 kDa. This discrepancy is likely due to the glycosylation state of Endolyn, which appears as a doublet of 78 kDa by western blotting despite a predicted molecular mass of 19 kDa (Ihrke et al., 2000). Endo-ShrmC cells were assayed for alterations in cellular morphology following induction by assessing the distribution of ZO-1 and E-cadherin. While control cells exhibit a normal columnar appearance (Fig. 3E), induced Endo-ShrmC cells exhibit dramatic alteration in apical morphology and tight junction architecture (Fig. 3F). Consistent with results from transient transfection, Endo-ShrmC-expressing cells display apical constriction. Quantification of Endo-ShrmC constriction was performed using the mixing experiments described above (not shown). In these mixed populations, Endo-ShrmC-expressing cells, neighboring wild-type cells and isolated wild-type cells had basal areas of approximately the same size ($131 \pm 18.4 \mu\text{m}^2$, $123 \pm 10.5 \mu\text{m}^2$ and $128 \pm 14 \mu\text{m}^2$, respectively). By contrast, the apical surfaces showed marked differences in area (Endo-ShrmC, $25.3 \pm 5 \mu\text{m}^2$; neighboring cells, $183.6 \pm 15.6 \mu\text{m}^2$; and isolated wild type, $128.5 \pm 21 \mu\text{m}^2$). These results indicate that the C-terminus of Shrm, when targeted to the apical compartment, is sufficient to cause constriction.

Endo-ShrmC expression also causes the formation of finger-like structures that extend across or into neighboring cells (arrows, Fig. 3F,H) and renders the AJC fragmented and filamentous in appearance (insets, Fig. 3F). Comparison of individual confocal sections from lateral or apical positions indicates the activity of Endo-ShrmC is restricted to the apical domain of the cell (Fig. 3G,H). Two possible scenarios could account for the formation of the finger like structures. First, these could be projections similar to filopodia. Second, these could be portions of the AJC complex that get left behind as a



cell constricts its apical surface. The differences in activity between ShrmL and Endo-ShrmC are likely due to the fact that ShrmL and Endo-ShrmC are localized to different portions of the cells and are acting on different populations of F-actin and not because they utilize different mechanism (see below). Also, Endo-ShrmC could be more active than ShrmL, either because more Endo-ShrmC gets to the apical membrane or because Endo-ShrmC has lost some form of regulation that limits ShrmL function.

ShrmL and Endo-ShrmC reorganize apical populations of F-actin in MDCK cells

Since the actin cytoskeleton is a critical regulator of epithelial cell shape and morphology, cells expressing ShrmL or Endo-ShrmC were assayed for changes in their apical cytoskeletal architecture by staining to detect F-actin and ZO-1. In control cells there is a population of F-actin loosely associated with AJC and a diffuse population of cortical F-actin associated with the apical plasma membrane (Fig. 4A). In cells expressing ShrmL there are alterations in the population of F-actin

associated with the AJC, such that the actin appears to be more condensed and closely associated with ZO-1 distribution (Fig. 4B).

Endo-ShrmC expression stimulates significant reorganization of the apical actin cytoskeleton, such that the cortical actin cytoskeleton is transformed into a complex array of actin stress fibers (Fig. 4C). This apical actin network appears to have two distinct forms depending on the morphology of the cell. The first is characterized by the presence of an apically positioned actin ring with radiating actin fibers extending toward the plasma membrane and terminating in tight junctions (arrowhead, Fig. 4C). These structures are typically seen in cells undergoing constriction and express higher levels of Endo-ShrmC (inset, Fig. 4C). The second population of F-actin is seen in cells that have increased their apical area to compensate for cells undergoing apical constriction. These cells possess apical stress fibers that traverse the apical dimensions of the cell perpendicular to the apical-basal axis and terminate at the AJC (arrows, Fig. 4C).

The above changes in cytoskeletal architecture reflect the observed changes in tight junction morphology seen following

ShrmL and Endo-ShrmC expression. The increased F-actin associated with tight junctions in ShrmL-expressing cells might account for their more rigid appearance. Similarly, the fragmented tight junctions seen in Endo-ShrmC-expressing cells might be caused by contraction of the actin filaments in the apical domain of the cell (Fig. 4C). The differences in actin architecture induced by ShrmL and Endo-ShrmC likely reflect the notion that these proteins utilize different populations of actin. Specifically, ShrmL is restricted to the AJC and probably acts on actin that is associated with the AJC. Conversely, Endo-ShrmC is localized to the entire apical surface and may act to reorganize apical cortical actin. Neither ShrmL nor Endo-ShrmC changes the organization of the basal actin cytoskeleton (not shown). Taken together, these data indicate that Shrm can induce alterations in the actin cytoskeleton in a spatially restricted manner and that these changes in cytoskeletal organization coincide with the observed alterations in cell morphology.

Apical constriction requires an intact actin cytoskeleton and the activities of myosin II and Rock

Shrm-induced alteration in apical cellular architecture is accompanied by reorganization of F-actin. Because non-muscle myosin II is a major regulator of actin-dependent contraction and morphological events in various types of non-muscle cells, the role of myosin II in apical constriction was assessed. Induced ShrmL cells were grown on Transwell filters for 48 hours, treated with the myosin II inhibitor blebbistatin (Straight et al., 2003) and stained to detect ZO-1 and Shrm. Treatment of induced ShrmL and Endo-ShrmC cells with DMSO has no effect on the Shrm-mediated changes in apical architecture (Fig. 5C,D). By contrast, treatment with blebbistatin reverts the constriction phenotype caused by ShrmL or Endo-ShrmC (Fig. 5E,F). Blebbistatin treatment also causes the apical actin cytoskeleton to revert to its normal organization (not shown). Importantly, treatment with blebbistatin does not alter the distribution of either ShrmL or Endo-ShrmC. These results indicate that myosin II activity is required for Shrm-induced apical constriction. Rock-I and II are upstream regulators of non-muscle myosin II activity (Chrzanowska-Wodnicka and Burridge, 1996). In other systems, inhibition of Rock often abrogates cellular processes that are dependent on myosin II (Hirose et al., 1998). Treatment of ShrmL- and Endo-ShrmC-expressing cells with the Rock inhibitor Y-27632 mimics blebbistatin treatment (Fig. 5G,H). Drug treatment has no effect on the morphology or the apical area of control cells (Fig. 5A,B). To quantify the effects of both blebbistatin and Y27632, mixing experiments were performed as described above. Both drugs restore the apical areas of ShrmL and Endo-ShrmL to dimensions similar to those of control cells (ShrmL/bleb, $123.5 \pm 21 \mu\text{m}^2$; ShrmL/Y27632, $119.2 \pm 32 \mu\text{m}^2$, Endo-ShrmC/bleb, $115.6 \pm 31 \mu\text{m}^2$; Endo-ShrmC/Y27632, $120.4 \pm 18 \mu\text{m}^2$; wild-type/bleb, $128.4 \pm 23 \mu\text{m}^2$; wild-type/Y27632, $130 \pm 19 \mu\text{m}^2$). These data

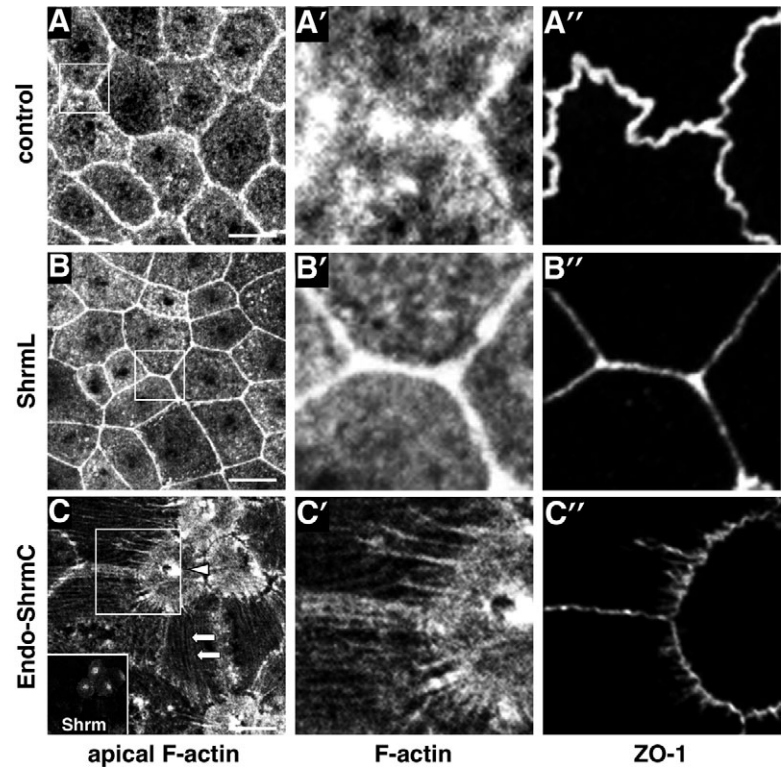


Fig. 4. Shrm-induced changes in morphology are associated with alterations in the organization of the apical actin cytoskeleton. (A-C) Control (A), induced ShrmL (B), or induced Endo-ShrmC (C) cells were grown on filters and stained to detect F-actin (A-C, A'-C') and ZO-1 (A''-C''). Boxed regions in A-C are enlarged in A'-C' and A''-C''. Inset in (C) shows Endo-ShrmC expression. Arrowhead denotes actin rings and arrows denote apical actin fibers. Images are projections of $0.2 \mu\text{m}$ sections spanning the AJC and apical plasma membrane. In all panels, scale bar represents $15 \mu\text{m}$.

indicate that ShrmL requires myosin II and Rock activity to elicit constriction and that the Endo-ShrmC protein causes constriction in a manner that is analogous to ShrmL.

Because Rock is activated by the GTP-bound form of the small GTPase Rho, the role of Rho in Shrm-mediated constriction was tested. Expression of wild-type RhoA in induced ShrmL cells results in a more severe constriction phenotype (Fig. 5J) while expression in un-induced cells has minimal affect on cell morphology (Fig. 5I). Surprisingly, expression of dominant-negative RhoA (RhoA19N) does not block constriction (Fig. 5K). These results are consistent with those observed in *Xenopus* embryos in which dominant-negative Rho does not abrogate Shrm-induced apical constriction (Haigo et al., 2003). These results suggest the Rho-Rock complex and Shrm might work in separate pathways that work together to mediate constriction. Alternatively, the activity of Rock may be limiting in this biological process. The activity of myosin II can also be regulated by MLCK. However, treatment of Endo-ShrmC-expressing cells with the MLCK inhibitor ML-7 ($40 \mu\text{M}$) has no effect on apical constriction (not shown).

To address the role of F-actin in apical constriction, ShrmL or Endo-ShrmC-expressing cells were treated with increasing concentrations of cytochalasin D (CD) for 30 minutes and then

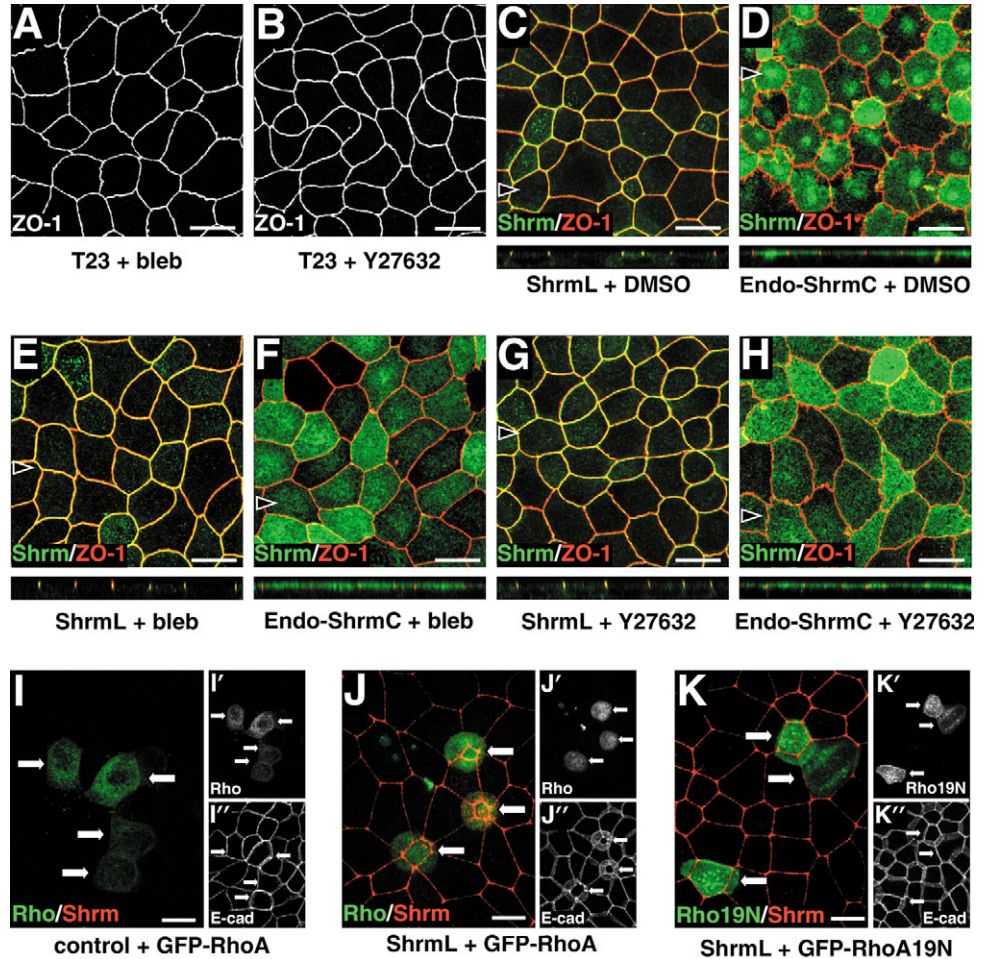


Fig. 5. The activity of myosin II and Rock are required for Shrm-induced cell shape changes. (A,B) Control cells were treated with blebbistatin (bleb) or Y27632 and stained to detect ZO-1. (C-H) Induced ShrmL cells (C,E,G) or Endo-ShrmC cells (D,F,H) were treated with DMSO (C and D), 100 μ M blebbistatin (E and F), or 10 μ M Y-27632 (G,H) and stained to detect Shrm (green) and ZO-1 (red). Arrowheads denote positions of the X-Z projections shown beneath each panel.

(I-K) Control cells (I) or ShrmL-expressing cells (J and K) were transfected with expression vectors for either GFP-RhoA (I and J) or GFP-RhoA19N (K) and stained to detect GFP, Shrm and E-cadherin. Merged images (I-K) show GFP (green) and ShrmL (red). Individual fluorescent signals for GFP (I'-K') and E-cadherin (I''-K'') are included. Arrows indicate transfected cells. In all panels, scale bar represents 15 μ m.

stained to detect ZO-1 to evaluate the extent of apical constriction. Surprisingly, treatment of cells expressing ShrmL with 1 μ M CD had minimal impact on apical constriction or tight junction morphology relative to DMSO treatment (Fig. 6A versus 6B). By contrast, treatment of Endo-ShrmC cells with 1 μ M CD causes significant phenotypic reversion relative to DMSO treatment (Fig. 6C versus 6D). One explanation for these disparate results is that ShrmL and Endo-ShrmC utilize distinct populations of F-actin to elicit morphological changes, each with different susceptibility to CD. Specifically, ShrmL appears to utilize the actin cytoskeleton already associated with the AJC while Endo-ShrmC induces the formation of a new network of apical actin stress fibers. Analysis of the basal and apical cytoskeletons in MDCK cells following CD treatment supports this hypothesis, as basal stress fibers and apical cortical actin disassemble following CD treatment while the actin associated with the AJC remains intact (Fig. 6E,F). Since the F-actin network induced by Endo-ShrmC is more reminiscent of basal stress fibers, this population of actin may be more sensitive to CD than that utilized by ShrmL to regulate apical constriction.

Increasing the concentration of CD to 2 μ M causes a more severe constriction phenotype and results in disruption of the epithelial monolayer (Fig. 6G-I). Control cells exhibit a mostly normal morphology following 2 μ M CD treatment (Fig. 6G). By contrast, monolayers of cells expressing either

ShrmL (Fig. 6H) or Endo-ShrmC (Fig. 6I) have clusters of Shrm-positive cells that are highly constricted (Fig. 6H,I) while the neighboring cells are stretched and have lost junctional integrity, as indicated by ZO-1 staining (Fig. 6H,I). These observations, in conjunction with the previous results regarding F-actin distribution and the requirements of myosin II activity, suggested that this disruption results from excessive cell stretching in the apical plane. In the absence of CD this does not occur because stretched cells use their cytoskeleton to oppose the pulling force exerted by constricting cells. This counter force could be lost following CD treatment. If this is true, inhibiting myosin II activity should eliminate the phenotype caused by 2 μ M CD treatment. This is the case, as blebbistatin ameliorates the phenotype caused by CD (Fig. 6J-L). These data indicate that Shrm regulates apical architecture through the activity of myosin II and the actin cytoskeleton.

Shrm regulates myosin II distribution in MDCK cells

The above results suggested that Shrm could control apical constriction by regulating the distribution of myosin II. To test this, control and induced cells were stained to detect myosin II-B and ZO-1. Un-induced cells show a small amount of myosin II-B localized to the AJC (Fig. 7A). By contrast, both ShrmL and Endo-ShrmC cells elicit redistribution of myosin

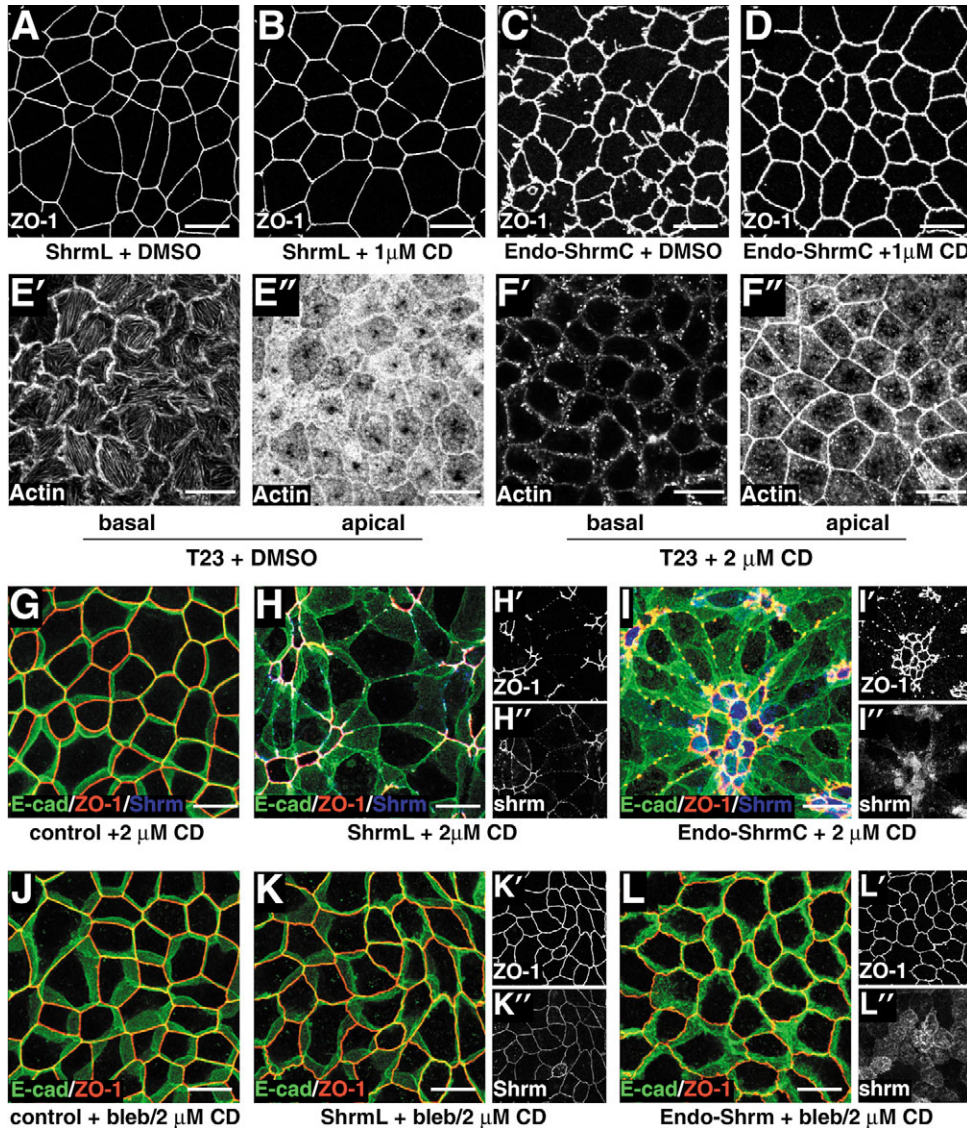


Fig. 6. The role of F-actin in Shrm-induced constriction. (A-D) Cells expressing ShrmL (A and B) or Endo-ShrmC cells (C and D) were treated with DMSO (A and C) or 1 μ M cytochalasin D (B and D) for 30 minutes and stained to detect ZO-1. (E,F) Wild-type T23 cells grown on Transwell filters were treated with DMSO (E' and E'') or 2 μ M CD (F' and F'') for 30 minutes, stained with phalloidin to detect F-actin and imaged by confocal microscopy to visualize the cytoskeleton at either the apical or basal surface. (G-I) Control (G), ShrmL expressing (H), or Endo-ShrmC expressing (I) cells were treated with 2 μ M cytochalasin D for 30 minutes and stained to detect E-cadherin (green), ZO-1 (red, H' and I'), or Shrm (blue, H'' and I''). (J-L) Control (J), ShrmL expressing (K), or Endo-ShrmC expressing (L) cells were pre-treated with 100 μ M blebbistatin for 30 minutes followed by 2 μ M cytochalasin D for 30 minutes and stained to detect E-cadherin (green), ZO-1 (red, K' and L'), or Shrm (blue, K'' and L''). Scale bar represents 15 μ m in all panels.

II-B to regions of the cell that reflect the localization of either ShrmL or Endo-ShrmC. In ShrmL-expressing cells, myosin II-B co-localizes with ZO-1 (Fig. 7B). Unlike ShrmL, which is uniformly distributed in the AJC, myosin II-B is seen in regularly spaced puncta. In Endo-ShrmC-expressing cells, myosin II-B is found in a filamentous array spanning the apical domain of the cell (Fig. 7C). To verify that Shrm acts autonomously to control myosin II distribution, wild type and ShrmL-expressing cells were mixed, plated on Transwell filters in the absence of doxycyclin and stained to detect either myosin II-B and ZO-1 (Fig. 7D) or myosin II-B, ZO-1 and ShrmL (Fig. 7E). Only cells that have constricted apical surfaces exhibit redistribution of myosin II-B into the AJC (Fig. 7D,E). The localization of myosin II-B in the AJC is coincident with both the distribution of F-actin and ShrmL in the AJC (Fig. 7F,G). Non-muscle myosin II is active when the associated RMLC is phosphorylated. To verify that the myosin II-B seen in ShrmL cells is active, induced cells were stained to detect RMLC phosphorylated on serine 18 and threonine 19 (pp-RMLC). Consistent with the distribution of myosin II-B,

pp-RMLC is detected in the tight junctions of ShrmL cells (Fig. 7H).

The average distance between individual myosin II puncta in ShrmL cells is approximately 600 nm, a distance consistent with the size of the sarcomeric repeat associated with contractile populations of F-actin in non-muscle cells (Peterson et al., 2004). To determine if the myosin II-B observed in the AJC of ShrmL-expressing cells represents a contractile unit, the distribution of myosin II-B relative to that of α -actinin, a marker for the sarcomeric repeat of actin stress fibers (Peterson et al., 2004), was assessed. ShrmL cells where grown on Transwell filters in the absence of doxycyclin, transiently transfected with an expression vector for GFP- α -actinin, and stained to detect myosin II-B and GFP- α -actinin. In cells expressing ShrmL, α -actinin and myosin II-B are distributed in a complementary, non-overlapping pattern in the AJC (Fig. 7I). Apical redistribution of α -actinin and pp-RMLC is also seen in Endo-ShrmC-expressing cells (data not shown). These data suggest that ShrmL, via ASD2, is capable of facilitating the formation of a contractile actomyosin

network in vivo and this network can alter cellular morphology.

Shrm is required for proper myosin IIB distribution during neural tube closure

Shrm mutant embryos display defects in cranial and trunk neural tube morphogenesis. In the cranial region, the neural tube fails to close, while in the spinal region, neural tube closure is completed but the neural folds are undulating, and the roof plate and central lumen are poorly formed (Hildebrand and Soriano, 1999). The observed ability of *Shrm* to regulate

myosin II distribution in vitro and the known requirement of actin in neural tube closure suggested that the phenotype of *Shrm*-deficient mice might stem from mislocalization of myosin II in the neural epithelium. To address this possibility, cryosections of e9.25 wild type and *shrm*-mutant embryos were stained to detect non-muscle myosin II-B and β -catenin and assayed by confocal microscopy. In wild-type embryos myosin II-B is enriched at the AJC in both the cranial and spinal neuroepithelium (Fig. 8A,B). This distribution is similar or identical to that of *Shrm* (Fig. 1). A significant proportion of myosin II-B staining is lost from this apical position in *shrm* mutant embryos (Fig. 8C,D). Fluorescent intensity of myosin

II staining across the apical surface of the *Shrm* null animals is 2-3 fold lower than in wild-type animals. This loss of myosin distribution appears specific as Nectin-3 and ZO-1 still localize to the sub-apical complex in the absence of *Shrm* (data not shown). These data suggest that *Shrm* functions to facilitate the sub-apical distribution of non-muscle myosin II-B, which, in turn, regulates the tissue rigidity and cell shape changes required to elaborate neural tube closure.

Discussion

The role of cell shape changes during the course of neural tube closure is an area of great interest due to the relatively high frequency of neural tube defects in human embryos (Copp et al., 1990b; Golden and Chernoff, 1995). *Shrm* is required for neurulation in both *Xenopus* and mouse embryos, and participates in this process by causing cells to undergo apical constriction (Haigo et al., 2003; Hildebrand and Soriano, 1999). *Shrm* is expressed throughout the neural epithelium and is localized to the AJC in neural epithelial cells. This complex is enriched in proteins that regulate cellular polarity, cell adhesion and cytoskeletal organization (Okabe et al., 2004; Takekuni et al., 2003). In the neural tube, this complex also contains F-actin and myosin II-B. It is presumably this apically positioned actomyosin complex that facilitates the cell shape changes that are required for generating the dorsal lateral hinge points and for providing the tissue rigidity that is necessary for

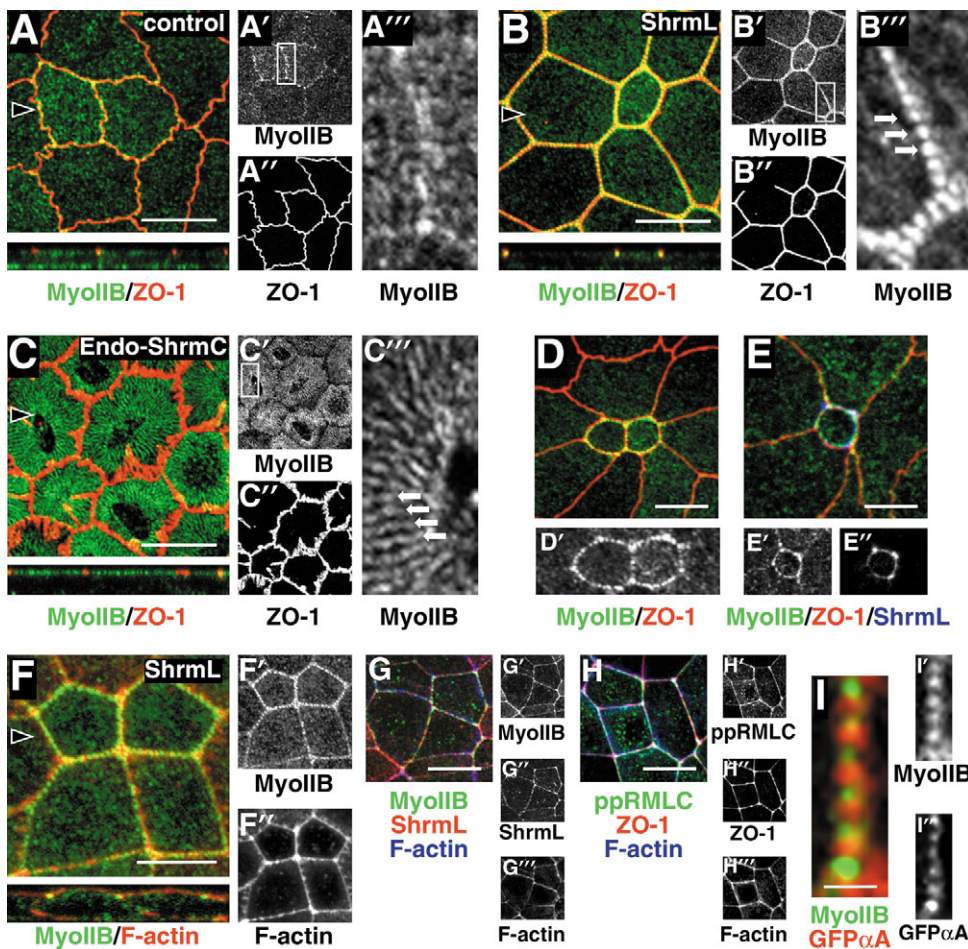


Fig. 7. *Shrm* alters the distribution of myosin II in MDCK cells. (A-C) Control (A), *ShrmL*-expressing (B) and *Endo-ShrmC*-expressing (C) cells were grown on filters and stained to detect non-muscle myosin II-B (green, A'-C', A'''-C''') and ZO-1 (red, A''-C''). Images are projections of 0.2 μ m optical sections that span the AJC and apical plasma membrane. Areas boxed in A'-C' are shown enlarged in A'''-C'''. Lower panels represent X-Z projections of the entire apical-basal axis. Arrowheads denote where X-Z sections were generated. Arrows denote the regularly spaced distribution of non-muscle myosin II-B. (D,E) Mixed populations of wild-type T23 cells and *ShrmL* cells were grown on filters in the absence of doxycyclin and stained to detect myosin II-B (green, D' and E') and ZO-1 (red) or myosin IIB, ZO-1 and *ShrmL* (blue, E''). (F) Induced *ShrmL* cells were stained to detect myosin II-B (green) and F-actin (red). Arrowhead denotes position of X-Z projection shown beneath panel. F' and F'' show myosin IIB and F-actin signals alone. (G) Induced *ShrmL* cells were stained to detect myosin IIB (green, G'), *ShrmL* (red, G'') and F-actin (blue, G'''). (H) Induced *ShrmL* cells grown on coverslips were stained to detect pp-RMLC (green, H'), ZO-1 (red, H'') and F-actin (blue, H'''). (I) Induced *ShrmL* cells were transiently transfected with a GFP- α -Actinin expressing vector and stained to detect myosin II-B (red, I') and GFP (green, I''). Scale bar equals 15 μ m in A-H and 1.5 μ m in I.

the large-scale tissue movements that must occur to successfully execute neural tube closure (Colas and Schoenwolf, 2001; Schoenwolf et al., 1988; Ybot-Gonzalez and Copp, 1999). Based on the ability of Shrm to cause the redistribution of non-muscle myosin II, the phenotypes of *shrm* mutant embryos and the loss of myosin II distribution in *shrm* mutants, it appears that Shrm-dependent localization of myosin II plays a critical role in correct morphogenesis of both the cranial and spinal neural tube.

The mechanism by which Shrm influences actomyosin distribution is unclear. The interaction does not appear to be direct, as complexes between ShrmL or Endo-ShrmC and myosin II have not been detected and, at least in vitro, the localization of actomyosin is overlapping with, but not identical to, that of ShrmL. Thus, the C-terminal domain of Shrm seems to act through other cellular proteins to influence the behavior of the actin cytoskeleton. A possible model for how Shrm functions to regulate neural tube closure is presented in Fig. 8E. Shrm is localized in the AJC of all neuroepithelial cells during neurulation, suggesting that an apical actomyosin network is needed to generate forces that cause cell shape changes in bending regions (a, Fig. 8E) and maintain tension across the apical surface in non-bending regions (b, Fig. 8E). Regardless of whether cells are constricting or not, Shrm directs assembly of an actomyosin network in the AJC and provides a contractile force around the circumference of each neural epithelial cell (c, Fig. 8E). Within each individual cell, Shrm is recruited to the AJC via either a direct interaction with actin or another AJC-resident protein and the C-terminal domain acts to recruit myosin II (d, Fig. 8E). There are several mechanisms by which recruitment could be regulated. Shrm, acting either directly or through a second cellular protein, could alter the properties of F-actin, rendering it a better substrate for myosin II-B and allowing for assembly of a contractile actomyosin complex. Alternatively, Shrm could act via another cellular protein that functions to regulate directly the activity or distribution of myosin II. Results to date indicate that Rock functions in parallel to maintain a population of active myosin. Once in the AJC, myosin II acts to contract the actin ring to generate cell shape changes or intercellular tension.

Recent evidence has demonstrated a critical role for apically positioned myosin II activity in several developmental processes of *Drosophila* and mice that involve the movement and morphogenesis of polarized epithelia, including convergent extension during germ band extension (Bertet et al., 2004), invagination of ectoderm (Nikolaidou and Barrett, 2004) and the movements of epithelial sheets (Shimizu et al., 2005). In the ventral ectoderm, myosin II (encoded by *zipper*) localizes to apical junctions in cells that are changing the orientation of their apical adhesion complexes (Bertet et al., 2004). This distribution and cellular phenotype is reminiscent of what is

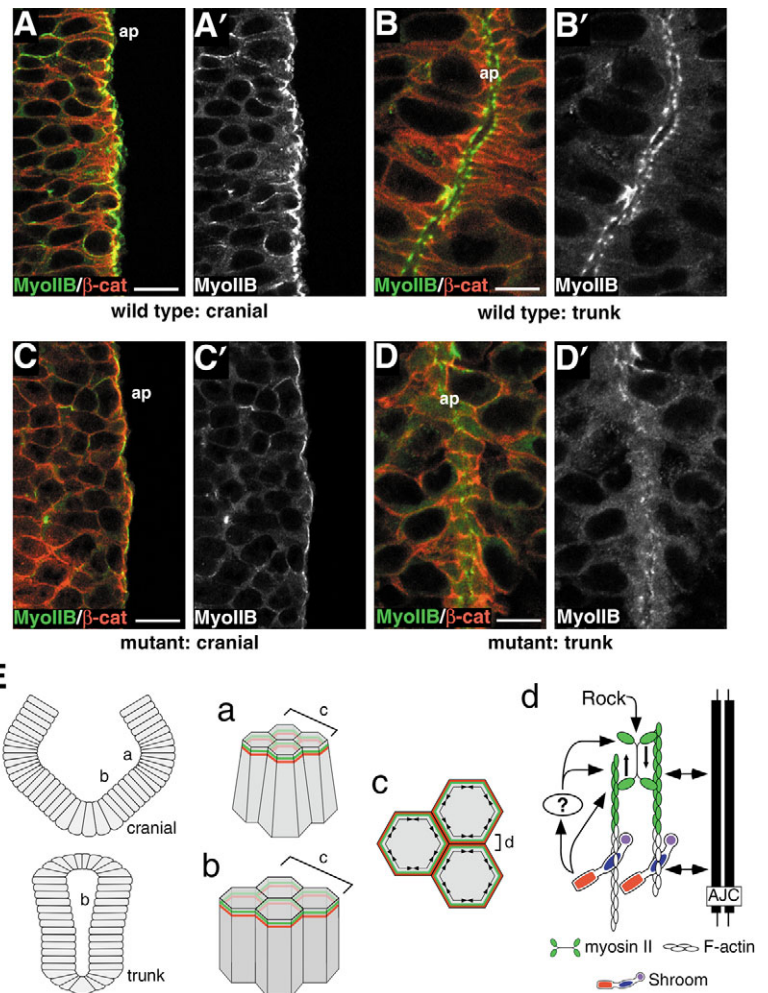


Fig. 8. Shrm is required for proper myosin IIB distribution during neural tube closure. (A-D) Cryosections of wild type (A and B) or *shrm* mutant (C and D) e9.25 mouse embryos were stained to detect non-muscle myosin II-B (green, A'-D') and β -catenin (red). Panels A and C show sections through the cranial neural folds while B and D are sections through the trunk neural tube. Scale bar equals 15 μ m, ap, apical surface. (E) Model of Shrm function in neural tube closure. Shown are schematics of the neural tube in both cranial and trunk regions indicating the presence of bending (a) and non-bending (b) regions of the cranial and trunk neural tube. Cells in both types of regions contain contractile rings (c) in the AJC that provide force around the circumference of the cell to mediate either apical constriction or provide tension. (d) Shrm is recruited to the AJC via either F-actin that is already localized there or another protein in the AJC (double head arrows). Once in the AJC complex, the C-terminal domain of Shrm facilitates the assembly of a contractile actomyosin complex (green actin and myosin). The C-terminus of Shrm could act directly or through a second cellular protein (?) to facilitate formation of the complex. It is predicted that Rock could be needed in parallel to maintain a population of active myosin II.

observed in MDCK cells expressing ShrmL, which change their apical geometry and lose or gain neighbors as a result of these adaptations in shape. Similarly, Zipper is localized to the apical plasma membrane and facilitates apical constriction as a way of changing tissue architecture and driving invagination of ectodermal placodes (Nikolaidou and Barrett, 2004). This is similar to how Shrm might function during hinge point formation in the neural tube. In the case of placode

morphogenesis, localized cell shape changes are accomplished by the spatially restricted activation of Rho1 via dRhoGEF2 and Concertina (Nikolaidou and Barrett, 2004). Interestingly, activation of this pathway in *Drosophila* S2 cells (Rogers et al., 2004) results in cell shape changes reminiscent of those caused by Shrm expression in MDCK cells. The requirement for Rock-I regulation of myosin II during vertebrate development has been assessed using gene targeting in mice. Embryos lacking Rock-I have defects in closure of the eyelids and ventral body wall, both of which involve the movement of polarized sheets of cells over a surface. These phenotypes stem from the inability of the polarized epithelia to assemble contractile actin cables (Shimizu et al., 2005). Similar to the above processes in flies and mice outlined above, Shrm appears to be necessary and sufficient to determine the spatial distribution of contractile actomyosin networks to initiate changes in tissue morphogenesis. Shrm-mediated constriction requires Rock and cooperates with Rho, but it does not appear to require Rho. This suggests that the Rho-Rock complex and Shrm may work in separate but convergent pathways, such that Shrm directs that distribution of myosin II, but that a population of the myosin II is maintained in an active state primarily by Rock, however other pathways might be able to compensate when Rho activity is blocked. Thus, Shrm may represent a novel pathway for controlling the distribution of activated myosin II in neural epithelial cells during development.

The ability of Shrm to regulate myosin II distribution both in vivo and in vitro indicate that Shrm is a critical determinant of epithelial cell shape during neural tube closure and a key step at which the process is regulated. Future experiments aimed at identifying the upstream and downstream components of these Shrm-controlled changes in cellular morphology should provide critical insights into understanding the relationship between cell shape and elaboration of the vertebrate body plan.

I thank the following investigators for generously providing reagents: Carol Otey, for GFP- α -actinin, David Hackam for GFP-RhoA and GFP-RhoA19N, Gerard Apodaca for T23 MDCK cells and Ora Weisz for the Endolyn cDNA. The mAb CMII 23 developed by G. W. Conrad was obtained from the Developmental Studies Hybridoma Bank developed under the auspices of the NICHD and maintained by The University of Iowa, Department of Biological Sciences, Iowa City, IA, 52242. Thanks also to Deborah Chapman, Jeffrey Brodsky, and lab members for critical reading and discussion of this manuscript. I also acknowledge Christine Konrad for technical support. This work was supported by grant NIH-GM67525 to J.D.H.

References

- Apodaca, G., Katz, L. A. and Mostov, K. E. (1994). Receptor-mediated transcytosis of IgA in MDCK cells is via apical recycling endosomes. *J. Cell Biol.* **125**, 67-86.
- Barth, A. I., Pollack, A. L., Altschuler, Y., Mostov, K. E. and Nelson, W. J. (1997). NH2-terminal deletion of beta-catenin results in stable colocalization of mutant beta-catenin with adenomatous polyposis coli protein and altered MDCK cell adhesion. *J. Cell Biol.* **136**, 693-706.
- Bertet, C., Sulak, L. and Lecuit, T. (2004). Myosin-dependent junction remodelling controls planar cell intercalation and axis elongation. *Nature* **429**, 667-671.
- Bresnick, A. R. (1999). Molecular mechanisms of nonmuscle myosin-II regulation. *Curr. Opin. Cell Biol.* **11**, 26-33.
- Brouns, M. R., Matheson, S. F., Hu, K., Delalle, I., Caviness, V. S., Silver, J., Bronson, R. T. and Settleman, J. (2000). The adhesion signaling molecule p190 RhoGAP is required for morphogenetic processes in neural development [In Process Citation]. *Development* **127**, 4891-4903.
- Campbell, L. R., Dayton, D. H. and Sohal, G. S. (1986). Neural tube defects: a review of human and animal studies on the etiology of neural tube defects. *Teratology* **34**, 171-187.
- Cetin, S., Ford, H. R., Sysko, L. R., Agarwal, C., Wang, J., Neal, M. D., Baty, C., Apodaca, G. and Hackam, D. J. (2004). Endotoxin inhibits intestinal epithelial restitution through activation of Rho-GTPase and increased focal adhesions. *J. Biol. Chem.* **279**, 24592-24600.
- Chrzanowska-Wodnicka, M. and Burridge, K. (1996). Rho-stimulated contractility drives the formation of stress fibers and focal adhesions. *J. Cell Biol.* **133**, 1403-1415.
- Colas, J. F. and Schoenwolf, G. C. (2001). Towards a cellular and molecular understanding of neurulation. *Dev. Dyn.* **221**, 117-145.
- Copp, A. J., Brook, F. A., Estibeiro, J. P., Shum, A. S. and Cockcroft, D. L. (1990a). The embryonic development of mammalian neural tube defects. *Prog. Neurobiol.* **35**, 363-403.
- Copp, A. J., Brook, F. A., Estibeiro, J. P., Shum, A. S. and Cockcroft, D. L. (1990b). The embryonic development of mammalian neural tube defects. *Prog. Neurobiol.* **35**, 363-403.
- Golden, J. A. and Chernoff, G. F. (1995). Multiple sites of anterior neural tube closure in humans: evidence from anterior neural tube defects (anencephaly). *Pediatrics* **95**, 506-510.
- Haigo, S. L., Hildebrand, J. D., Harland, R. M. and Wallingford, J. B. (2003). Shroom induces apical constriction and is required for hinge-point formation during neural tube closure. *Curr. Biol.* **13**, 2125-2137.
- Hayashi, T. and Carthew, R. W. (2004). Surface mechanics mediate pattern formation in the developing retina. *Nature* **431**, 647-652.
- Hildebrand, J. D. and Soriano, P. (1999). Shroom, a PDZ domain-containing actin-binding protein, is required for neural tube morphogenesis in mice. *Cell* **99**, 486-497.
- Hirose, M., Ishizaki, T., Watanabe, N., Uehata, M., Kranenburg, O., Moolenaar, W. H., Matsumura, F., Maekawa, M., Bito, H. and Narumiyama, S. (1998). Molecular dissection of the Rho-associated protein kinase (p160ROCK)-regulated neurite remodeling in neuroblastoma N1E-115 cells. *J. Cell Biol.* **141**, 1625-1636.
- Ihrke, G., Gray, S. R. and Luzio, J. P. (2000). Endolyn is a mucin-like type I membrane protein targeted to lysosomes by its cytoplasmic tail. *Biochem. J.* **345**, 287-296.
- Ihrke, G., Bruns, J. R., Luzio, J. P. and Weisz, O. A. (2001). Competing sorting signals guide endolyn along a novel route to lysosomes in MDCK cells. *EMBO J.* **20**, 6256-6264.
- Koleske, A. J., Gifford, A. M., Scott, M. L., Nee, M., Bronson, R. T., Miczek, K. A. and Baltimore, D. (1998). Essential roles for the Abl and Arg tyrosine kinases in neurulation. *Neuron* **21**, 1259-1272.
- Lanier, L. M., Gates, M. A., Witke, W., Menzies, A. S., Wehman, A. M., Macklis, J. D., Kwiatkowski, D., Soriano, P. and Gertler, F. B. (1999). Mena is required for neurulation and commissure formation. *Neuron* **22**, 313-325.
- Menzies, A. S., Aszodi, A., Williams, S. E., Pfeifer, A., Wehman, A. M., Goh, K. L., Mason, C. A., Fassler, R. and Gertler, F. B. (2004). Mena and vasodilator-stimulated phosphoprotein are required for multiple actin-dependent processes that shape the vertebrate nervous system. *J. Neurosci.* **24**, 8029-8038.
- Nelson, W. J. (2003). Adaptation of core mechanisms to generate cell polarity. *Nature* **422**, 766-774.
- Nikolaidou, K. K. and Barrett, K. (2004). A Rho GTPase signaling pathway is used iteratively in epithelial folding and potentially selects the outcome of Rho activation. *Curr. Biol.* **14**, 1822-1826.
- Okabe, N., Ozaki-Kuroda, K., Nakanishi, H., Shimizu, K. and Takai, Y. (2004). Expression patterns of nectins and afadin during epithelial remodeling in the mouse embryo. *Dev. Dyn.* **230**, 174-186.
- Peterson, L. J., Rajfur, Z., Maddox, A. S., Freel, C. D., Chen, Y., Edlund, M., Otey, C. and Burridge, K. (2004). Simultaneous stretching and contraction of stress fibers in vivo. *Mol. Biol. Cell* **15**, 3497-3508.
- Redowicz, M. J. (2001). Regulation of nonmuscle myosins by heavy chain phosphorylation. *J. Muscle Res. Cell Motil.* **22**, 163-173.
- Rogers, S. L., Wiedemann, U., Hacker, U., Turck, C. and Vale, R. D. (2004). *Drosophila* RhoGEF2 associates with microtubule plus ends in an EB1-dependent manner. *Curr. Biol.* **14**, 1827-1833.
- Schoenwolf, G. C., Folsom, D. and Moe, A. (1988). A reexamination of the role of microfilaments in neurulation in the chick embryo. *Anat. Rec.* **220**, 87-102.

- Shimizu, Y., Thumkeo, D., Keel, J., Ishizaki, T., Oshima, H., Oshima, M., Noda, Y., Matsumura, F., Taketo, M. M. and Narumiya, S.** (2005). ROCK-I regulates closure of the eyelids and ventral body wall by inducing assembly of actomyosin bundles. *J. Cell Biol.* **168**, 941-953.
- Smith, J. L. and Schoenwolf, G. C.** (1997). Neurulation: coming to closure. *Trends Neurosci.* **20**, 510-507.
- Straight, A. F., Cheung, A., Limouze, J., Chen, I., Westwood, N. J., Sellers, J. R. and Mitchison, T. J.** (2003). Dissecting temporal and spatial control of cytokinesis with a myosin II Inhibitor. *Science* **299**, 1743-1747.
- Stumpo, D. J., Bock, C. B., Tuttle, J. S. and Blackshear, P. J.** (1995). MARCKS deficiency in mice leads to abnormal brain development and perinatal death. *Proc. Natl. Acad. Sci. USA* **92**, 944-948.
- Takekuni, K., Ikeda, W., Fujito, T., Morimoto, K., Takeuchi, M., Monden, M. and Takai, Y.** (2003). Direct binding of cell polarity protein PAR-3 to cell-cell adhesion molecule nectin at neuroepithelial cells of developing mouse. *J. Biol. Chem.* **278**, 5497-5500.
- Thumkeo, D., Keel, J., Ishizaki, T., Hirose, M., Nonomura, K., Oshima, H., Oshima, M., Taketo, M. M. and Narumiya, S.** (2003). Targeted disruption of the mouse rho-associated kinase 2 gene results in intrauterine growth retardation and fetal death. *Mol. Cell. Biol.* **23**, 5043-5055.
- Vaezi, A., Bauer, C., Vasioukhin, V. and Fuchs, E.** (2002). Actin cable dynamics and Rho/Rock orchestrate a polarized cytoskeletal architecture in the early steps of assembling a stratified epithelium. *Dev. Cell* **3**, 367-381.
- Vogelmann, R. and Nelson, W. J.** (2005). Fractionation of the epithelial apical junctional complex: reassessment of protein distributions in different substructures. *Mol. Biol. Cell* **16**, 701-716.
- Wei, L., Roberts, W., Wang, L., Yamada, M., Zhang, S., Zhao, Z., Rivkees, S. A., Schwartz, R. J. and Imanaka-Yoshida, K.** (2001). Rho kinases play an obligatory role in vertebrate embryonic organogenesis. *Development* **128**, 2953-2962.
- Xu, W., Baribault, H. and Adamson, E. D.** (1998). Vinculin knockout results in heart and brain defects during embryonic development. *Development* **125**, 327-337.
- Ybot-Gonzalez, P. and Copp, A. J.** (1999). Bending of the neural plate during mouse spinal neurulation is independent of actin microfilaments. *Dev. Dyn.* **215**, 273-283.